Articles

Fragment Reconstitution of a Small Protein: Disulfide Mutant of a Short C-Terminal Fragment Derived from Streptococcal Protein G†

Naohiro Kobayashi,‡ Shinya Honda,§ and Eisuke Munekata*,‡

Institute of Applied Biochemistry, University of Tsukuba, Tsukuba 305-8572, Japan, and National Institute of Bioscience and Human-Technology, Tsukuba 305-8566, Japan

Received July 23, 1998; Revised Manuscript Received January 12, 1999

ABSTRACT: Hierarchical studies on the folding of protein G B1 domain have shown that the C-terminal fragment (C16) has a considerable amount of β-hairpin structure that exchanges between the folded and unfolded states at room temperature, and that the C16 fragment binds noncovalently to an N-terminal fragment (N40) under physiological conditions. Those studies have led us to the hypothesis that the amphipathic β-hairpin structure of C16 initiates folding of the domain. To obtain a more detailed understanding of the folding mechanism of the domain, we designed a mutant of C16 (SS16ox) with a disulfide bond between residues 41 and 56, and then examined the interaction of the mutant with N40 by surface plasmon resonance (SPR) and by thermal denaturation studies using circular dichroism. SS16ox strongly interacted with N40, with an equilibrium constant, K_D, that was 7-fold higher than wild-type. The association rate constant, k_{on}, of SS16ox was 8.7-fold higher than that of wild-type. This strong interaction can be explained by the entropic effect of the disulfide bond. The introduction of the disulfide bond into C16 stabilizes the β-hairpin structure of C16, accelerates the association rate with N40, and then stabilizes the whole complex. These results support a hypothetical folding mechanism of protein G where the amphipathic β-hairpin structure of C16 acts as a nucleus and accelerates folding of the whole molecule.

The immunoglobulin binding domain of protein G is a cell wall protein of groups C and G streptococci (*1, 2*). The B1 domain of protein G (56 amino acid residues) shows a high heat denaturation temperature (close to 360 K) and possesses a peculiar folding topology (*3, 4*). Hierarchical studies on the folding of protein G showed that the C-terminal fragment, C16,[1] has a nativelike β-hairpin structure in aqueous solution (*5, 6*), and that the two fragments corresponding to sequences 1−20 and 21−40, respectively, contain a nativelike β-hairpin structure and an α-helical structure in 30% trifluoroethanol (*7, 8*). We have investigated the interaction between the N-terminal fragment of 40 residues, N40, and C16 utilizing CD, NMR (*9*), and differential scanning calorimetry (*10*). In those studies, we demonstrated that one hydrophilic and three aromatic interactions cooperatively participate in the folding of the amphipathic β-hairpin structure of C16, and that these interactions are also important for the stability of the noncovalent complex between C16 and N40. These results led us to the hypotheses that the amphipathic β-hairpin structure of C16 initiates and accelerates the folding of N40. Although we demonstrated that C16 noncovalently binds to N40 to reconstitute a native conformation of the domain, the kinetics of this interaction are still unknown. Therefore, the development of a routine analyzing system to assess the interaction between the wild-type and mutant fragments would provide us detailed information for the folding of protein G. Although a wide variety of methods for evaluating protein−protein or protein−ligand interactions have been developed, it is difficult to precisely elucidate peptide−peptide interactions. The reasons for this are (i) the specific

† This work was supported by a research grant from the Special Research Project on Circulation Biosystems, University of Tsukuba, by Grant-in Aid for Scientific Research 08760111 from the Ministry of Education, Japan, and by a fellowship (to N.K.) from the Japan Society for the Promotion of Science.

* To whom correspondence should be addressed at the Institute of Applied Biochemistry, University of Tsukuba, Tsukuba 305-8572, Japan. E-mail: munekata@sakura.cc.tsukuba.ac.jp. Telephone: +81-298-53-4606. Fax: +81-298-53-6277.

‡ Institute of Applied Biochemistry, University of Tsukuba.

§ National Institute of Bioscience and Human-Technology.

[1] Abbreviations: C16, C-terminal fragment corresponding to the sequence of protein G B1 domain (41−56); N40, N-terminal fragment corresponding to the sequence of protein G B1 domain (1−40); CD, circular dichroism; NMR, nuclear magnetic resonance; SPR, surface plasmon resonance; SS16ox, oxidated form of [Csy^{41}, Cys^{56}, Lys^{57}]-C16; SS16red, reduced form of [Csy^{41}, Cys^{56}, Lys^{57}]-C16; Fmoc, 9-fluorenylmethoxycarbonyl; NMP, *N*-methylpyrrolidone; DCC, 1,3-dicyclohexylcarbodiimide; DIEA, *N*,*N*-diisopropylethylamine; TFA, trifluoroacetic acid; EDT, ethanedithiol; HPLC, high-performance liquid chromatography; TSP, sodium 3-trimethylsilylpropionate-d_4; K_D, equilibrium affinity constant; k_{on}, association rate constant; k_{off}, dissociation rate constant; T_m, transition temperature; ΔH, change in enthalpy from folded to unfolded state; ΔG, change in Gibbs free energy from folded to unfolded state; ΔC_p, change in heat capacity from folded to unfolded state.

10.1021/bi981777w CCC: $18.00 © 1999 American Chemical Society
Published on Web 02/26/1999

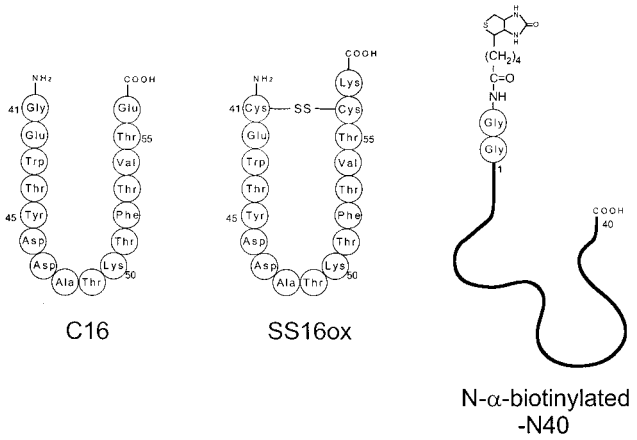

FIGURE 1: Structures of the peptides used in this study. For *N*-α-biotinylated-N40, the sequence from residues 1 to 40 is represented by a thick line.

peptide−peptide interaction is small compared to the nonspecific interaction, and (ii) the difference in molecular mass between the bound and free peptides is too small to use size-dependent techniques such as gel chromatography, dialysis, and ultracentrifugation. This barrier to the study of small peptide−peptide interactions was recently overcome by the advent of surface plasmon resonance (SPR) which has solved the problems associated with the study of small peptide−peptide interactions. The SPR technique is adequate for analysis of small peptides with the low binding affinity interactions observed between N40 and C16. In the present study, we investigated the kinetics of the interaction between N40 and two mutants of C16, one with a disulfide bond between residues 41 and 56 (SS16ox) and one with the same mutation but reduced (SS16red), by SPR. The stabilities of the complexes were also examined by thermal denaturation measurements using circular dichroism in aqueous solution. By comparison with the same analysis for the pair of wild-type sequence, we discussed the folding mechanism of the B1 domain of protein G.

EXPERIMENTAL PROCEDURES

Design of the Disulfide Mutant of C16. We found eight possible sites for introducing a disulfide bond using the following criteria: (i) the site should be exposed to solvent; (ii) the introduced disulfide bond should not perturb the main-chain conformation of the domain. The structures of the complex of the disulfide mutants and N40 were generated by deleting and inserting atoms and bonds on the structure of protein G B1 domain (Brookhaven Protein Data Bank 2GB1) using NMRgraf program (Molecular Simulations Inc.) on an Indigo 4000 workstation (Silicon Graphics Co. Ltd.). The obtained structures were subjected to the following calculations: (i) 500 steps of energy minimization; (ii) 10 ps of molecular dynamics at 600 K; (iii) 500 steps of energy minimization. The deviations for the conformational energies and the coordination of the conformers were compared with those of the wild-type domain, and then a mutant which showed the smallest values was chosen for this study.

Synthesis of Peptides. All peptides described in this report (Figure 1) were synthesized using the conventional solid-phase method combined with a manual synthesis protocol that we established. For *N*-α-biotinylated-N40, after the elongation of two additional glycine residues on the N40 peptide, the biotinylation of the N-terminus was achieved in NMP by addition of biotine, DCC, and DIEA in 10-fold excess. After elongation of the full length of the peptide, the resins were treated with 20% piperidine for 20 min, followed by TFA−H_2O−EDT (9.5:0.25:0.25) treatment for 1 h. The obtained crude peptides were purified by preparative reverse-phase HPLC using an Inertsil ODS-2 column (25 × 250 mm, GL-Science). The reduced form of SS16ox was oxidized in 50 mM Tris-HCl buffer, pH 8.5, containing 1 mM oxidized glutathione and 0.1 mM reduced glutathione for 24 h, and then similarly purified by preparative reverse-phase HPLC. The homogeneity of the purified peptides was confirmed by analytical reverse-phase HPLC using a Wakosil 5C18 column (4.6 × 250 mm). The amino acid components were analyzed with a Hitachi L-8500 amino acid analyzer, the sequences with a Shimazu PPSQ-10 amino acid sequencer, and the molecular mass with a JEOL JMS-HX110HF double-focusing mass spectrometer. The concentrations of the peptides were determined using the molar extinction coefficients for tryptophan and tyrosine in model compounds (*11*).

In Situ Reduction of SS16ox. The measurements of ^{1}H NMR, SPR, and CD for SS16red were achieved by addition of solid dithiothreitol corresponding to 30 mM in the sample of SS16ox, and incubating for 10 min. The completion of the reduction was confirmed by analytical reverse-phase HPLC.

NMR Experiments. Samples for NMR measurements were prepared by dissolving the peptides in 99.996% D_2O. These sample solutions contained 5 mM sodium phosphate buffer, pH 7.0. All signals were referenced relative to the HDO signal, which was previously calibrated with a small amount of TSP (sodium 3-trimethylsilylpropionate-d_4) as a reference for 0 ppm. The pH values of the solutions were adjusted to an accuracy of ±0.02 by titration with DCl or NaOD using a glass microelectrode without correction for the isotope effect. All 1D spectra (500.130 MHz) were measured at 296 K using a Bruker DMX500 spectrometer. The acquired free induction decays were commonly 16K data points with 16 scans, which were zero-filled into 32K data points by multiplying the shift sine-bell function squared prior to Fourier transformation.

Surface Plasmon Resonance (SPR) Analysis. Peptide−peptide interaction studies were performed using a Pharmacia Biosensor BIAcore instrument (*12*, *13*). SA5 research grade sensor chips (Pharmacia Biosensor) were used for all experiments on which 65 ng/mm^2 of streptoavidin was preimmobilized. The peptide was immobilized by injection of 100 μg/mL *N*-α-biotinylated-N40 solutions of 5 mM sodium phosphate buffer, pH 7.0, to a SA5 sensor chip at a flow rate of 5 μL/min (293 K). Under these conditions, typically 800 RU (corresponding to about 200 fmol of peptide/mm^2) were immobilized.

All measurements used 5 mM sodium phosphate buffer, pH 7.0, as a running buffer, except for SS16red for which the buffer contained 30 mM dithiothreitol. Although the sensor chip surface was not regenerated after each cycle, the sensorgrams showed small base line drifting (within ±2.0 RU/min) and high reproducibility due to the low affinity of all injected peptides to *N*-α-biotinylated-N40. Samples of C16 and mutants in a range of concentrations were injected

over *N*-α-biotinylated-N40 at a constant flow rate of 10 μL/min.

BIACore Binding Kinetics. Association and dissociation rate constants were calculated by nonlinear fitting of the primary sensorgram data (*14*, *15*) using the program BIAevaluation version 2.1 (Pharmacia Biosensor). For nonlinear analysis, association rate constants, k_{on}, were derived from the binding phase of the sensorgrams. Briefly, the slope of each sensorgram, d*R*/d*t*, was plotted against the response, *R*, and the slope of this line in turn plotted against the analyte concentration, *C*. The association rate constant is obtained directly from the gradient of this second plot:

$$dR/dt = k_{on}(R_{max} - R)C - k_{off}R \quad (1)$$

Dissociation rate constants were derived from the phase after the injected pulse of sample by plotting $\ln(R_0/R_t)$ against time, where R_0 and R_t are the response at an arbitrary starting time and at time *t*, respectively.

Both association and dissociation rate constants were also obtained from linear transformation of the sensorgram data and the equation:

$$k_s = k_{on}C + k_{off} \quad (2)$$

where k_s is the slope of the d*R*/d*t* versus *R* plot. A range of concentrations are analyzed, and a plot of k_s versus *C* has a slope of k_{on} and a *y*-intercept of k_{off}. Equilibrium affinity constants, K_D, were derived from the ratio of association and dissociation constants, k_{off}/k_{on}.

Thermal Denaturation for N40+C16, N40+SS16ox, and N40+SS16red by Circular Dichroism. The model for the thermal denaturation of N40+C16 in a state of equilibrium between the associated and dissociated peptides was established elsewhere (*10*). According to the model, K_D is simply expressed with f_d as the fraction of the denaturation (or the dissociation) state and C_t as the total concentration of N40 or C16; then

$$K_D = \frac{f_d^2}{1 - f_d} C_t \quad (3)$$

The equilibrium constant K_D is also introduced from the van't Hoff equation:

$$K_D = \frac{C_t}{2} \exp\left\{ -\frac{\Delta H_m}{RT}\left(1 - \frac{T}{T_m}\right) - \frac{\Delta C_p}{RT}\left(T - T_m - T \ln\left(\frac{T}{T_m}\right)\right)\right\} \quad (4)$$

where ΔH_m and ΔC_p are the changes in enthalpy and heat capacity, respectively, from the folded to unfold state at the transition temperature T_m. Therefore, the molecular ellipticity at 222 nm ($[\theta]_{222}$) is given by the equation:

$$[\theta]_{222} = [\theta]_{222,F} + \{[\theta]_{222,U} - [\theta]_{222,F}\} f_d \quad (5)$$

where $[\theta]_{222,F}$ and $[\theta]_{222,U}$ are the molecular ellipticity at 222 nm of the folded and the unfolded state, respectively.

The thermal denaturation of the equimolar mixtures (ca. 1 mM) of N40+C16, N40+SS16ox, and N40+SS16red in 5 mM sodium phosphate buffer (pH 7.0) was monitored by CD at 222 nm using cells with a path length of 0.02 cm on a JASCO J-600 spectropolarimeter equipped with a Haake F-3 temperature control unit. The temperature was increased at a linear rate of 0.5 deg/min.

RESULTS AND DISCUSSION

Many models have been proposed to understand why proteins fold so quickly. These include the diffusion−collision−adhesion model (*16*), the flame work model (*17*, *18*), the hydrophobic collapse model (*19*, *20*), and the nucleation condensation model (*21*). Based on the investigation of the protein G B1 domain, which used a hierarchical approach, we built a hypothetical folding pathway consisting of the following steps: (i) the C-terminal segment corresponding to C16 forms an amphipathic β-hairpin structure in the early folding stage, creating a stable hydrophobic surface; (ii) the N-terminal segment corresponding to N40 interacts with this surface; and (iii) the well-packed native structure is completed (*9*). We considered that the stability of the amphipathic β-hairpin structure should correlate with the folding rate of the domain. To further understand this aspect, we have tried to design an energetically stabilized C16 mutant which would be expected to accelerate domain folding.

Disulfide Bond of SS16ox. Introducing a disulfide bond into a peptide is the most conventional and straightforward way to design a stable mutant. Earlier studies have shown that introduction of artificial disulfides into proteins enhances protein stability by lowering the entropy of the unfolded state (*22*−*25*). However, in some cases, the packing or fluctuations of proteins have been perturbed by the introduction of an artificial disulfide bond due to the strain energy associated with disulfide bond formation in the folded state. Therefore, the disulfide bond should be exposed to solvent so as to avoid new interactions and repulsions in the designed protein. To find an energetically favored disulfide isomer of C16, we generated eight possible disulfide isomers of C16 which bind to N40 using a molecular simulation program, NMRgraf. Then the obtained structures and the designed peptides were subjected to molecular dynamics and energy minimization calculations. We selected a disulfide bond between Cys^{41} and Cys^{56}, because it showed nearly the same conformational energy as the wild-type domain in these calculations.

Conformations of Fragment Mixtures. First, to examine whether the mixture of C16 mutants and N40 forms a nativelike complex, we measured the 1D proton NMR spectrum of the mixtures. In our previous study, we have observed largely upfield and downfield signals in the aliphatic and α-proton regions, respectively, when the fragments efficiently form a nativelike complex (*9*). Even though the interaction between the C16 mutants and N40 is weak, we successfully observed the characteristic signals derived from the complex because of the low sensitivity of the NMR experiment (ca. 1 mM). Figure 2 shows the aliphatic regions of the 1D-NMR spectra of the mixtures N40+C16, N40+SS16ox, and N40+SS16red.

All of the spectra showed some extremely upfield signals in the aliphatic signal region, 0.5 to −1.5 ppm. Among them, two upfield shifted signals in the spectrum of the mixture N40+C16 have been assigned to $C_\beta H$ of Leu^5 and $C_\gamma H_3$ of Val^{54} previously (*9*). In the hydrophobic core of the complex, the $C_\beta H$ of Leu^5 and the $C_\gamma H_3$ of Val^{54} were strongly shielded

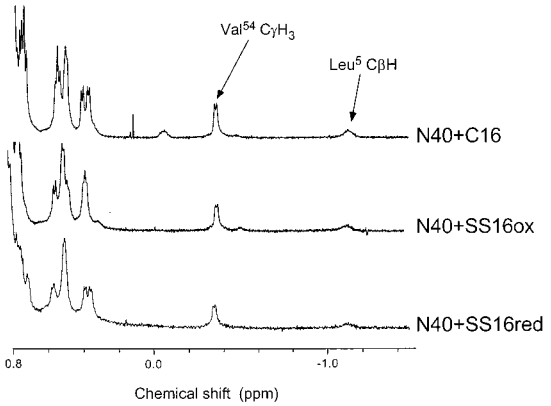

FIGURE 2: Aliphatic regions of 1D ^{1}H NMR spectra of the mixtures N40+C16, N40+SS16ox, and N40+SS16red in D_2O at pH 7.0 and 296 K. The sample concentration was ca. 1.0 mM. For the mixture N40+SS16red, the sample contained 30 mM dithiothreitol.

with the ring current from aromatic side chains of Trp[43] and Phe[30], respectively. Generally, some strongly upfield-shifted methyl or methylene signals are observed in the spectrum of a globular protein possessing a well-packed hydrophobic core, which is known to be sensitive to the altered orientation of the aromatic ring to methyl or methylene groups in the hydrophobic core. Therefore, the upfield signals, $C_\beta H$ of Leu[5] and $C_\gamma H_3$ of Val[54] should be a good indicator for evaluating the nativelike packing of the hydrophobic core of the complexes. As shown in Figure 2, the two signals appeared in the spectra of the complexes N40+SS16ox and N40+SS16red and showed nearly identical chemical shifts to those of wild-type complex. This indicates that the side-chain orientations of Trp[43] to Val[54] and of Phe[30] to Leu[5] are well conserved in the hydrophobic core of three complexes, suggesting that the complexes commonly form a nativelike hydrophobic core structure. Furthermore, CD spectra in the far-UV region of the three complexes showed a similar profile (data not shown) in which the values of the mean residue ellipticity at 222 nm at 278 K were -9.32×10^3, -7.79×10^3, and -8.33×10^3 deg·cm^2·dmol^{-1} for N40+C16, N40+SS16ox, and N40+SS16red complexes, respectively. These results indicate that the three complexes have similar secondary structures. Taken together with the 1D NMR results, the CD spectra indicate that the three complexes have nativelike structure, and that the artificial disulfide did not significantly affect the global domain conformation.

Surface Plasmon Resonances. To obtain kinetic information on the interaction between the C16 mutants and N40, we used the BIACore instrument (Pharmacia Biosensor AB), a biosensor-based analytical system which allows kinetic characterization of interactions between biomolecules in real time in a flow system (*13, 14*). This biosensor uses surface plasmon resonance (SPR) to monitor the binding of molecules immobilized on the sensor tip surface.

Figure 3 shows the association and dissociation profile of 50 μM C16 interacting with N40 immobilized on three different chip surfaces in 5 mM sodium phosphate, buffer pH 7.0 at 278 K, and shows the high reproducibility of our system. In contrast, the profile of a control experiment between C16 and the tip surface was the same as that of running buffer with N40, indicating the effects are completely negligible for the nonspecific interaction of 50 μM C16 with avidin. Figure 4 consists of sensorgrams showing the

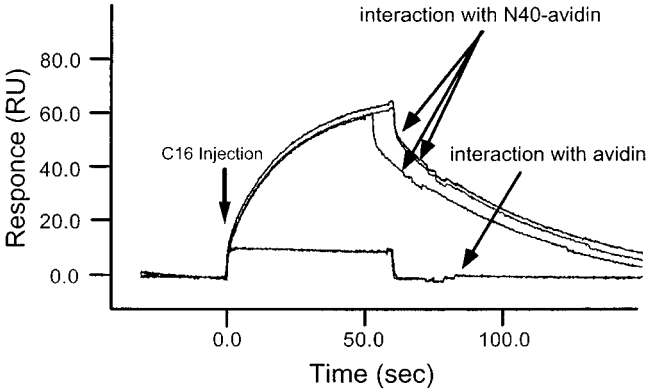

FIGURE 3: Sensorgrams showing 50 μM C16 binding to and dissociation from biotinylated N40 captured on preimmobilized avidin in 5 mM sodium phosphate buffer, pH 7.0 at 278 K.

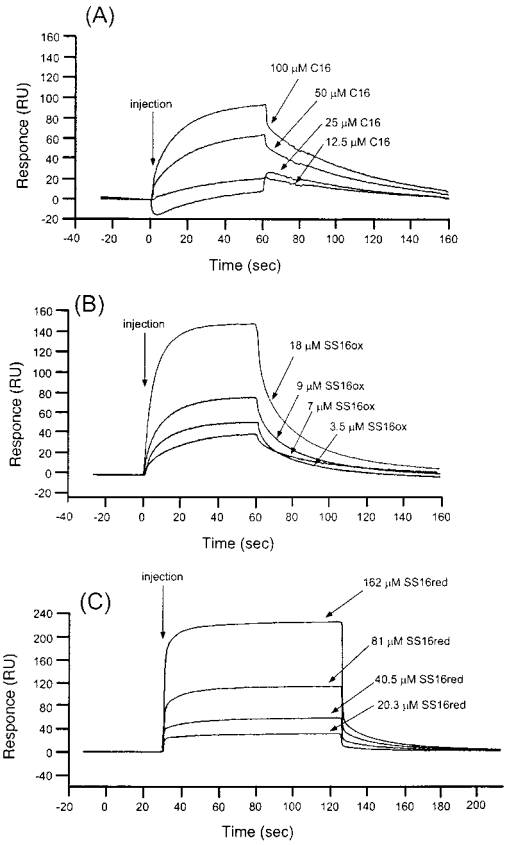

FIGURE 4: Relative response versus time for the binding to immobilized biotinylated N40 of the analytes C16 (A), SS16ox (B), and SS16red (C) in 5 mM sodium phosphate buffer, pH 7.0 at 278 K.

interaction of C16, SS16ox, and SS16red with biotinylated N40 in 5 mM sodium phosphate buffer, pH 7.0 at 278 K. The dissociation constants, k_{off}, of the peptides were obtained from nonlinear fitting as shown in Figure 5A. Using the obtained k_{off} values, the association constants, k_{on}, of the peptides were obtained as shown in Figure 5B. The resulting rate constants were similar to the values derived from linear analysis (see Figure 6 and Table 2), indicating that the rate constants were independent of peptide concentration in the experimental range. Values obtained from the BIACore kinetic analysis are listed in Table 1. The rate constants of SS16red were close to those of wild-type, indicating that changing Gly[41] and Glu[56] to Cys and elongation of C-terminal Lys did not affect the interaction between N40 and C16. An

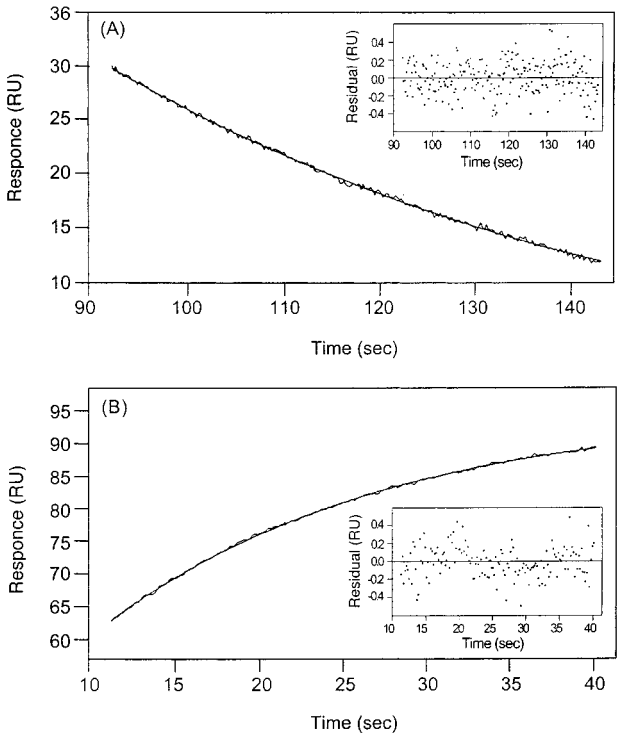

FIGURE 5: Curve fittings of C16 dissociation (A) and association (B) phases to BIAevaluation version 2.1 using a single-component model. Residuals for the fittings are represented in the insets.

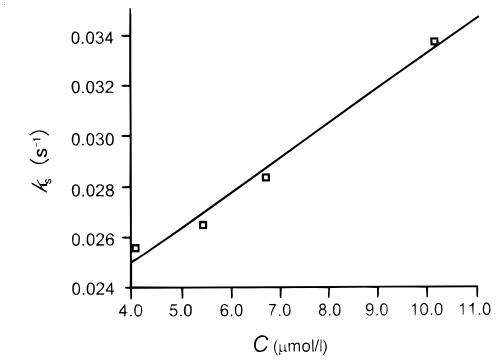

FIGURE 6: Linear regression analysis of k_s versus C plots for C16 on-rate determination. The slope of the plot yielded the k_{on} values derived from the experiments with varied concentration of C16.

8.7-fold increase was observed in the association constant for SS16ox relative to wild-type, while the dissociation constant values were similar for both peptides. This resulted in a 7-fold increase in the affinity constant, K_D^{SPR},, of SS16ox. Further discussion of these values is mentioned below.

Thermal Denaturation Using Circular Dichroism Melting Measurements. Thermal denaturation was also used to examine the unfolding behavior and stability of the complexes, N40+C16, N40+SS16ox, and N40+SS16red. For each complex, a cooperative transition was observed in circular dichroism melting measurements.

As mentioned above, the far-UV CD spectra of these three complexes were similar to each other. In addition, the spectra at high temperature were almost identical. The values of the mean residue ellipticity (deg·cm^2·dmol^{-1}) at 222 nm were -3.77×10^3 at 340 K, -3.51×10^3 at 350 K, and -3.60×10^3 at 340 K, respectively. These results indicate that the secondary structures of the three complexes in the associated/folded state as well as in dissociated/unfolded state are almost equivalent. To cancel out the errors in molecular ellipticity arising from the systematic uncertainty in the method for peptide concentration determination, all transition curves observed by circular dichroism melting measurements were normalized with each value in the associated or dissociated states (Figure 7). Since the interaction between peptides was not strong, we have expected that the association is always incomplete at the lowest temperature. Therefore, the value in the fully associated state was determined by using a variable parameter instead of a constant value in the calculation of the nonlinear least-squares fitting of eq 5 to the measured transition curves.

The transition curve for N40+SS16ox shifted to a higher temperature compared to that of the native pair, N40+C16, while the curve for N40+SS16red was almost identical. We performed a thermodynamic analysis of the data using an established model (*10*) to obtain parameters as listed in Table 2. For the complex N40+SS16red, the values of T_m, ΔC_p, and ΔG were not changed significantly. This indicates that there is no influence of the Cys replacement on stability, which was also shown in the SPR measurements described above. On the other hand, the stabilizing effect of disulfide bond formation was confirmed by the values of T_m and ΔG for N40+SS16ox (Table 2). Compared to the thermodynamic parameters of the wild-type complex, disulfide bond formation shows a decrease in enthalpy ($\Delta\Delta H < 0$). However, a large increase in entropy ($-T\Delta\Delta S > 0$) compensates for the enthalpic disadvantage and stabilizes the whole system ($\Delta\Delta G > 0$). Thus, the improvement in stability is explained by the entropic effect of the introduced disulfide bond between the N- and C-termini of C16.

Implication in Domain Folding. The equilibrium constants K_D^{SPR} and K_D^{CD}, for mutants and wild-type, obtained individually from SPR or CD measurements using eq 2 or 4, were converted into thermodynamic parameters, $\Delta\Delta G$, respectively, using the equation:

$$\Delta\Delta G(T) = RT \ln \frac{K_{D,mutant}}{K_{D,wild}} \quad (6)$$

Although SPR and CD melting experiments were performed at different temperatures, the differences of the $\Delta\Delta G$ values were small (Tables 1 and 2). This indicates that the immobilization of the peptide fragments on sensor tips in the SPR experiment does not significantly affect the evaluation of peptide association. Furthermore, the $\Delta\Delta G$ values of SPR and CD melting experiments were commonly positive, indicating that the introduction of a disulfide bond to C16 contributes to stabilization of fragment reconstitution.

How does the introduced disulfide bond stabilize the complex N40−SS16ox? The k_{off} values of the mutants and wild-type showed relatively small differences, while the k_{on} differences between SS16ox and SS16red, and SS16ox and C16 were much larger. To explain this discrepancy, we considered these kinetic values as thermodynamic information, and then tried to build a simple reaction profile consisting of the unfolded state, transition state, and unfolded state of the complexes. For the profile, we used an assumption in which the unfolded states of complexes N40+C16 and N40+SS16red and the folded states of complexes

Table 1: Interaction of C16, SS16ox, and SS16red with Biotinylated N40[a]

analyte peptide	k_{on}[b] (M^{-1} s^{-1})	k_{off}[b] (s^{-1})	K_D^{SPR}[c] (μM)	$K_D^{SPR}/K_D^{SPR}_{(wild)}$[d]	$\Delta\Delta G^{SPR}(278)$[e] (kJ/mol)
C16	446 ± 4.6 (402 ± 32.2)	0.0179 ± 0.0006 (0.0214 ± 0.0019)	40.1 (53.2)	–	–
SS16ox	3610 ± 380 (3420 ± 282)	0.0275 ± 0.0003 (0.0372 ± 0.0031)	7.6 (10.8)	0.19	3.8
SS16red	522 ± 15.4 (565 ± 9.2)	0.0279 ± 0.0004 (0.0254 ± 0.0008)	53.4 (44.9)	1.33	−0.67

[a] Conditions as described under Experimental Procedures. The values in parentheses are obtained from linear data analysis according to eq 2. [b] k_{on} and k_{off} values were obtained from nonlinear data analysis according to eq 1. [c] K_D^{SPR} is the ratio of k_{on} to k_{off}. [d] $K_D^{SPR}/K_D^{SPR}_{(wild)}$ is the ratio of $K_D^{SPR}(278)$ of the disulfide mutants to that of the complex of the wild pair, N40+C16. [e] $\Delta\Delta G(278)$ are the differences in ΔG between the disulfide mutants and the complex N40+C16 at 278 K, using eq 6.

Table 2: Thermodynamic Parameters for the Complexes N40+C16, N40+SS16ox, and N40+SS16red[a]

sample	concn (mM)	T_m (K)	ΔH_m (kJ/mol)	ΔC_p [kJ/(mol·deg)]	$K_D^{CD}(320)$[b] (μM)	K_D^{CD}/K_D^{CD} (wild)[c]	$\Delta\Delta H(320)$[d] (kJ/mol)	$-T\Delta\Delta S(320)$[d] (kJ/mol)	$\Delta\Delta G^{CD}(320)$[d] (kJ/mol)
N40+C16	0.97	313	121	2.6	1390	1.00	–	–	–
N40+SS16ox	1.00	327	126	1.9	189	0.14	−25.1	30.4	5.3
N40+SS16red	1.00	313	135	2.6	1640	1.18	13.9	−14.4	−0.4

[a] Conditions as described under Experimental Procedures. [b] $K_D(320)$ is the equilibrium constant at 320 K. [c] K_D^{CD}/K_D^{CD}(wild) is the ratio of $K_D^{CD}(320)$ of the disulfide mutants to that of the complex of the wild pair, N40+C16. [d] $\Delta\Delta H(320)$, $T\Delta\Delta S(320)$, and $\Delta\Delta G(320)$ are the differences in ΔH, $T\Delta S$, and ΔG, respectively, between the disulfide mutants and the complex N40+C16 at 320 K.

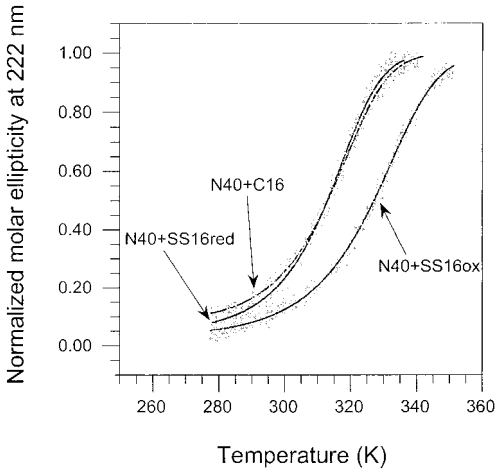

FIGURE 7: Thermal denaturation of the complexes N40+C16, N40+SS16ox, and N40+SS16red as measured by circular dichroism melting experiments at 222 nm. The equimolar mixtures of the fragments were dissolved in 5 mM sodium phosphate buffer (pH 7.0). Shaded dots indicate experimental data at the 0.5 K/min heating rate. Solid lines show theoretical curves best fitted to eqs 3, 4, and 5 using a nonlinear least-squares method.

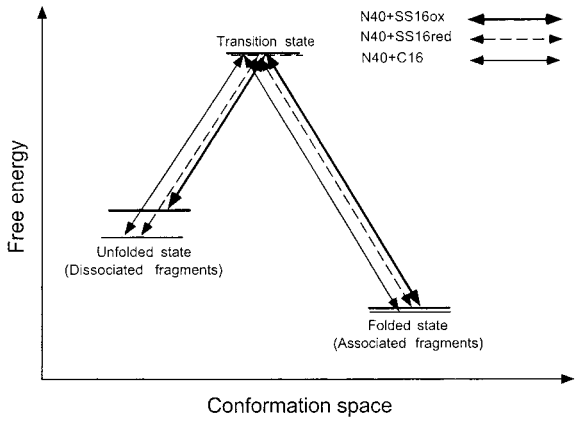

FIGURE 8: A representative explanation for the folding transition of the mixtures N40+C16, N40+SS16ox, and N40+SS16red. The rate constants obtained from the SPR experiments are taken into account on the energy levels.

N40+SS16ox and N40+SS16red are on a similar energy level, respectively. This assumption is supported by the facts that the complexes N40+SS16ox and N40+SS16red possess a nearly similar conformation and also that the introduction of Cys residues in the C16 fragment does not significantly change the contribution of entropy or enthalpy in the dissociated/unfolded state of complexes N40+C16 and N40+SS16red. The reaction profiles of the association between the peptides would be illustrated as shown in Figure 8. The energy levels of unfolded, transition, and folded states were estimated from the resultant values derived from SPR experiments. Considering the principle of SPR analysis (*26*), there are some limitations for deducing values of the free energy of the transition states as the experiments in solution, so that the estimated energy values and scales on the free energy axis should not be shown. Given that limitation, the reaction profiles obviously give us the interpretation that the $\Delta\Delta G$ values mainly contribute to the unfolded state of the complex. As mentioned above, the introduction of a disulfide bond affects both the entropic and enthalpic thermodynamic terms of the thermal unfolding. However, the net value of the energy term, $\Delta\Delta G$, was positive owing to the large contribution of the entropic effect. Therefore, it is concluded that the introduction of the disulfide bond stabilized the complex N40+SS16ox by decreasing the entropy of the unfolded state of C16, thereby increasing the energy level of the unfolded state of the complex.

In this study, the results support our hypothetical folding pathway of protein G, in which stabilization of the nativelike β-hairpin of the C16 segment in the early folding stages accelerates the domain folding. We also consider the mutant SS16ox to be a good model for more advanced studies on the structural features of the β-hairpin intermediate. We have built a routine assessment system for investigating the interaction between N40 and C16 mutants using a combination of NMR, SPR, and CD. Undoubtedly, the system is a

powerful tool that can be used to explore the folding of small proteins with low-affinity interaction between fragments. Our system may also prove useful in the design of more stable protein.

ACKNOWLEDGMENT

We thank Dr. Y. Ishibashi and Ms. H. Yoshida, Takeda Chemical Industries Ltd., for measurements of FAB mass spectroscopy.

REFERENCES

1. Sjöbring, U., Björck, L., and Kastern, W. (1991) *J. Biol. Chem. 266*, 399−405.
2. Fahnestock, S. R., Alexander, P., Nagle, J., and Filpula, D. (1986) *J. Bacteriol. 167*, 870−880.
3. Gronenborn, A. M., Filpula, D. R., Essig, N. Z., Achari, A., Whitlow, M., Wingfield, P. T., and Clore, G. M. (1991) *Science 253*, 657−661.
4. Gallagher, T., Alexander, P., Bryan, P., and Gilliland, G. L. (1994) *Biochemistry 33*, 4721−4729.
5. Kobayashi, N., Endo, S., and Munekata, E. (1992) in *Peptide Chemistry 1992* (Yanaihara, N., Ed.) pp 278−280, ESCOM, Leiden, The Netherlands.
6. Blanco, F. J., Rivas, G., and Serrano, L. (1994) *Nat. Struct. Biol. 1*, 584−590.
7. Blanco, F. J., Jiménez, M. A., Pineda, A., Rico, M., Santoro, J., and Nieto, J. L. (1994) *Biochemistry 33*, 6004−6014.
8. Blanco, F. J., and Serrano, L. (1995) *Eur. J. Biochem. 230*, 634−649.
9. Kobayashi, N., Honda, S., Yoshii, H., Uedaira, H., and Munekata, E. (1995) *FEBS Lett. 366*, 99−103.
10. Honda, S., Kobayashi, N., Munekata, E., and Uedaira, H. (1999) *Biochemistry 38*, 1203−1231.
11. Gill, S. C., and von Hippel, P. H. (1989) *Anal. Biochem. 182*, 319−326.
12. Jönsson, U., Fägerstam, L., Ivarsson, B., Johnsson, B., Karlsson, R., Lundh, K., Löfås, S., Persson, B., Roos, H., Rönnberg, I., Sjölander, S., Stenberg, E., Ståhlberg, R., Urbaniczky, C., Östlin, H., and Malmqvist, M. (1991) *Bio-Techniques 11*, 620−627.
13. Malmqvist, M. (1993) *Nature 361*, 186−187.
14. Karlsson, R., Michaelsson, A., and Mattson, L. (1991) *J. Immunol. Methods*, *145*, 229−240.
15. Fägerstam, L., Frostell-Karlsson, Å., Karlsson, R., Persson, B., and Rönnberg, I. (1992) *J. Chromatogr. 597*, 397−410.
16. Karplus, M., and Weaver, D. L. (1976) *Nature 260*, 404−406.
17. Kim, P. S., and Baldwin, R. L. (1982) *Anuu. Rev. Biochem. 51*, 459−489.
18. Kim, P. S., and Baldwin, R. L. (1990) *Anuu. Rev. Biochem. 59*, 631−660.
19. Dill, K. A. (1985) *Biochemistry 24*, 1501−1509.
20. Dill, K. A., Fiebig, K. M., and Chan, H. S. (1993) *Proc. Natl. Acad. Sci. U.S.A. 90*, 1942−1946.
21. Itzhaki, L. S., Otzen, D. E., and Fersht, A. R. (1995) *J. Mol. Biol. 254*, 260−288.
22. Perry, L. J., and Wetzel, R. (1984) *Science 226*, 555−557.
23. Pantoliano, M. W., Landner, R. C., Bryan, P. N., Rollence, M. L., Wood, J. F., and Poulos, T. L. (1987) *Biochemistry 26*, 2077−2082.
24. Matsumura, M., Becktel, W. J., Levitt, M., and Matthews, B. W. (1989) *Proc. Natl. Acad. Sci. U.S.A. 76*, 6042−6046.
25. Kanaya, S., Katsuda, C., Kimura, S., Nakai, T., Kitakuni, E., Nakamura, H., Katayanagi, K., Morikawa, K., and Ikehara, M. (1991) *J. Biol. Chem. 266*, 6038−6044.
26. Karlsson, R., Roos, H., Fägerstam, L., and Persson, B. (1994) *Methods: Comp. Methods Enzymol. 6*, 99−110.

BI981777W